Appl Nanosci (2015) 5:553–561
DOI 10.1007/s13204-014-0349-7

ORIGINAL ARTICLE

Nickel nanoparticles embedded in carbon foam for improving electromagnetic shielding effectiveness

Rajeev Kumar · Saroj Kumari · Sanjay R. Dhakate

Received: 2 July 2014 / Accepted: 14 August 2014 / Published online: 29 August 2014

Abstract To improve electromagnetic shielding effectiveness of light weight carbon foam (CF), magnetic nanoparticles were embedded in it during processing. The CF was developed from the coal tar pitch and mixture of coal tar pitch-Nickel (Ni) nanoparticles by sacrificial template technique and heat treated to up 1,000 °C. To ascertain the effect of Ni nanoparticles embedded in CF, it was characterized by scanning electron microscopy, X-ray diffraction, Raman spectroscopy, vector network analyzer and vibration sample magnetometer. It is observed that Ni nanoparticles embedded in the carbon material play an important role for improving the structure and electrical conductivity of CF-Ni by catalytic carbonization. The structural investigation suggests that the Ni nanoparticles embedded in the carbon material in bulk as well on the surface of CF. The CF demonstrates excellent shielding response in the frequency range 8.2–12.4 GHz in which total shielding effectiveness (SE) dominated by absorption losses. The total SE is −25 and −61 dB of CF and CF-Ni, it is governed by absorption losses −48.5 dB in CF-Ni. This increase is due to the increase in dielectric and magnetic losses of ferromagnetic Ni nanoparticles with high surface area. Thus, light weight CF embedded with small amount of magnetic nanoparticles can be useful material for stealth technology.

Keywords Carbon foam · Nickel nanoparticles · Raman spectroscopy · Electromagnetic shielding effectiveness · Magnetization

R. Kumar · S. Kumari · S. R. Dhakate (✉)
Physics and Engineering of Carbon, Division of Material Physics and Engineering, CSIR-National Physical Laboratory, Dr. K. S. Krishnan Marg, 110012 New Delhi, India
e-mail: dhakate@mail.nplindia.org

Introduction

The increasing use of large number of wireless gadgets in contemporary technological world and related electromagnetic (EM) radiation is becoming a serious problem that disturbs stable working conditions of electronic appliances and may harm to human being (Chung 2000). In civil and military aerospace vehicles, protection from EM radiations as well as regulation of thermal heating of electronic power systems is necessary to protect them from any form of damages. In particular, light weight shielding and structural materials are needed to mitigate EM interference (EMI) from electronic systems and to protect human from hazards of space radiation, e.g., aerospace vehicles, especially in 8.2–12.4 GHz frequency region (X-band) (Coleman et al. 2006; Du et al. 2006). The EMI shielding refers to the reflection and absorption of electromagnetic radiation by a material, which thereby acts as shield against the penetration of radiation through the shield. Electrical conductor such as metal and carbon materials mainly shield by reflection of radiation. On the other hand, magnetic materials mainly used for absorption of the radiation. The most materials used for shielding are chosen due to their electrical conductivity rather than their magnetic behavior. While in certain application such as sheath technology, shielding materials have mandatory to absorb maximum EM radiation. The magnetic absorbers depend on the magnetic hysteresis effect, which is attained in magnetic materials such as ferrites. But densities of the magnetic materials are generally high and absorbing bandwidths for magnetic absorbers are usually narrow. On the other hand, dielectric materials are light weight, but do not match up to the absorptivity of magnetic absorbers (Seo et al. 2004; Park et al. 2006; Oh et al. 2004). These two types of materials have different advantages and

disadvantages when they are applied as absorbers. They can be used together as a composite, and the magnetic material is usually the base one, but high density of the material is still of great concern. Practically, an effective EMI shielding material being lightweight is an important requirement in aerospace transportation vehicles and space structures (Yang et al. 2005). The shielding effectiveness (SE) value should be >-50 dB in the X-band frequency (Wang et al. 2012). Among the different materials, carbon-based materials are comparatively light weight and structurally strong.

Carbon foam (CF) is a sponge-like rigid high-performance engineering materials in which carbon ligaments are interconnected to each other (Klett et al. 2000, 2004). Recently, it has attracted lot of attention owing to outstanding properties such as low density, large surface area with open cell wall structure, good thermal and mechanical stability (Gallego and Klett 2003; Inagaki et al. 2004).

There are different types of electromagnetic (EM) radiation shielding materials or RAM has been developed since after the advent of radar, but very few reports on the CF are available in literature. As discussed above, generally carbon is conducting materials in which SE is dominated by reflection losses that depend upon the processing temperature of CF and starting precursor.

Yang et al. (2004) reported the development of CF from mesophase pitch by foaming technique which is heated at temperature between 400 and 800 °C and studied its microwave (2–18 GHz) absorption characteristics. It is found that CF heat treated at 600 and 700 °C exhibits better microwave absorption (reflection loss 10 dB). Fang et al. (2006) reported the numerical prediction and experimental validation of CF as microwave (8.2–12.4 GHz) absorber. The CF is fabricated by traditional technique through the polymer foam replication method and it is heat treated at 700, 750 and 800 °C, and characterized them for microwave absorption. The reflection coefficient of 20 mm thick foam is in the order of 8–10 dB. Fang et al. (2007) have also studied the electromagnetic characteristics of CF having different pore size and electrical conductivities which are controlled by the carbonization temperature (700–760 °C). The electromagnetic parameters of these carbon foam and their corresponding pulverized powders are measured by a resonant cavity perturbation technique at a frequency of 2.45 GHz. The CF has dielectric loss several times larger than their corresponding pulverized powder. This suggests that low temperature heat treated foam EM-SE is dominated by absorption. Recently, Moglie et al. (2012) studied the EM-SE of CF (GRAFOAM FPA-20 and FRA-10) in the frequency band 1–4 GHz using the nested reverberation chamber method. It is reported that with increasing thickness of CF total SE increases. Micheli and Marcheti (2012) reported the effect of multi-walled carbon nanotubes epoxy resin mixture filled in the pores of CF and studied its role on EM radiation absorption properties of CF in frequency range 2–3 GHz. It is observed that absorption properties reaching peak of the reflection coefficient −45 dB for a normally incident plane wave. Blacker et al. (2008) reported that EM-SE greater than about 40 dB in the frequency range of 400 MHz–18 GHz of rigid porous electrically conductive CF is achieved by incorporating electrically conductive carbon nanofiber in a polymer matrix, which is used for the joining the CF enclosures. Blacker et al. (2011) reported that the development of electrically gradated CF material exhibits different electrical resistivity values at or near different surfaces of CF in which the electrical resistivity increases with increasing the thickness of foam and decreases with increasing processing temperature. These electrically gradated CF materials may be used as radar absorbers. But in the case of aerospace and military application, the shield material should have high SE which is mainly dominated by absorption losses as well thermal stability.

The carbon nanomaterials in combination with magnetic particles are used to improve EM radiation absorption and have become more intensive absorber as compared to carbon nanomaterials (Huang and Wu 2000; Liu et al. 2006; Che et al. 2004). Che et al. (2004, 2006) have reported that magnetic nanoparticles/carbon nanotubes (CNTs) exhibited improved microwave absorption properties because of their proper EM matching between the dielectric loss and the magnetic loss.

The purpose of this study is to improve the microwave absorption properties of carbon foam by the incorporation of magnetic nanoparticles. In the present work, CF is developed from a mixture of coal tar pitch and Ni nanoparticles by sacrificial template technique and then heat treated to 1000 °C. The results reveal that SE is dominated by EM radiation absorption mechanism rather than reflection mechanism in the Ni nanoparticle-embedded CF.

Experimental

Synthesis of nickel nanoparticles

The Ni nanoparticles were synthesized by the process reported literature (Saravanan et al. 2001). The 1 g of nickel chloride hexahydrate ($NiCl_2{\cdot}6H_2O$) was dissolved in 100-ml ethylene glycol. The solution was heated to 70–80 °C. Later on, 4.5-ml hydrazine hydrate was added to above solution for complete reduction. After 10 min, 3.0 g of NaOH (1 M) solution was added slowly in continuation of stirring. The complete solution was kept under magnetic stirrer for 1 h at 60 °C. After 1 h, reaction was completed and black nickel nanoparticles were formed. These

nanoparticles were collected, washed several times by ethanol and dried in the room temperature. The reduction reaction can be expressed as

$$2NiCl_2 + H_4N_2 + 4NaOH \rightarrow 2Ni^{+} + N_2 + 4H_2O + 4NaCl$$

It is seen that N_2 gas is continuously bubbled during the reaction and as results it automatically creates N_2 atmosphere throughout the reaction. Hence, no extra N_2 gas is required for the synthesis of nickel nanoparticles.

Fabrication of nickel nanoparticles incorporated carbon foam

Initially, coal tar pitch was modified with the nickel nanoparticles 1.0 wt% and heat treated at 400 °C for 25 h in inert atmosphere. The carbon foam was prepared by sacrificial template technique in which the polyurethane (PU) foam (density 0.030 g/cc and average pore size 0.45 mm) was used as template. The Ni nanoparticle-based modified pitch was grounded by ball milling in a tungsten carbide jar for about 5–6 h to get the particle size of mixture less than 30μm, so that these particles can easily penetrate inside the cells of PU foam. The above mixture was converted into water-based slurry (with 3 % polyvinyl alcohol) and it was impregnated inside pore of PU template foam by vacuum infiltration technique (Kumar et al. 2013a, b, c; Yadav et al. 2011). The impregnated PU foam was converted into carbon foam by series of heat treatments in air as well as in an inert atmosphere up to 1,000 °C. Initially, the modified coal tar pitch and Ni nanoparticles mixture impregnated PU foams were heat treated @ 1 °C min^{-1} up to 275 °C in the nitrogen atmosphere for 1 h followed by oxidation and stabilization in air atmosphere at temperature 300 °C. The stabilized foam was carbonized in tubular high temperature furnace at 1,000 °C with heating rate 10 °C h^{-1} in inert atmosphere. The schematic of process for synthesis of nickel nanoparticle-based CF is shown in Fig. 1. The CF is designated as CF and Ni nanoparticle-embedded CF as CF-Ni.

Characterization

Raman spectra of the CF and Ni-CF samples were recorded using Renishaw in via Raman spectrometer, UK with laser as an excitation source at 514 nm. The crystal structure of CF samples was studied by X-ray diffraction (XRD, D–8 Advanced Bruker diffractometer) using CuK_α radiation ($\lambda = 1.5418$ Å). The morphology of Ni nanoparticles was observed by transmission electron microscope (TEM, Tecnai, G20-Super-Twin, 300 kV). The TEM sample was prepared by Ni nanoparticle dispersed in solvent and put over the carbon-coated copper grid. The surface morphology of the CF samples was observed by scanning electron microscope (SEM, VP-EVO, MA-10, Carl-Zeiss, UK) operating at an accelerating potential of 10.0 kV. The electrical conductivity CF (size 60 × 20 × 4 mm) was measured as per standard ASTM C611-98. The dc four probe contact method was used in which a Keithley 224 programmable current source was used for providing current. The voltage drop was measured by Keithley 197A auto ranging digital microvoltmeter. The values reported in text are average of six readings of voltage drops at different places of the sample. The compressive strength of CF was

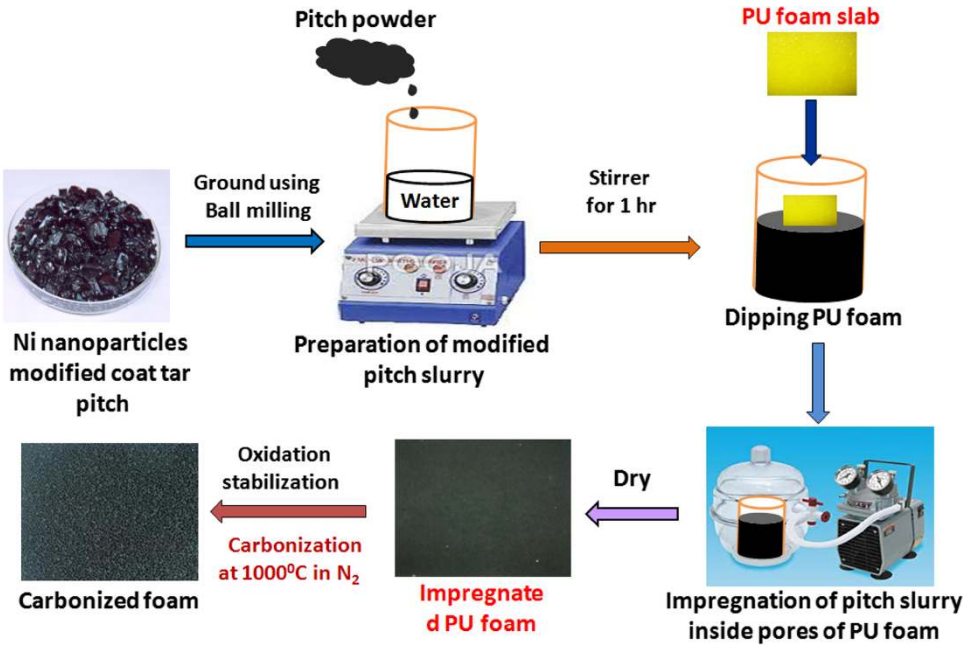

Fig. 1 Fabrication of Ni nanoparticle-embedded coal tar pitch-based carbon foam using sacrificial (PU foam) template technique

measured by Instron Universal Testing Machine, model 1122 as per ASTM C695-91. EM-SE and EM attributes (complex permittivity and permeability) were measured by waveguide using vector network analyzer (VNA E8263BAgilent Technologies). The rectangular samples (26 × 13 mm) of thickness 2.75 mm were placed inside the cavity of sample holder which matches the internal dimensions of X-band (8.4–12.4 GHz) wave guide. The sample holder was placed between the flanges of the waveguide connected between the two ports of VNA. The magnetic property of the CF samples was measured by vibration sample magnetometer (VSM) model 7304, Lakeshore Cryotronics Inc., USA with a maximum magnetic field of 1.2 T, using Perspex holder vibrating horizontally at frequency of 76 Hz.

Results and discussion

In Fig. 2a, TEM image of Ni nanoparticles shows that the particles are of different shape and size, particularly somewhat star or starfruit shaped and it looks like agglomerated form. The average size of Ni nanoparticles is in between 50 and 100 nm. Figure 2b shows the powder XRD patterns of the Ni nanoparticles. The nanoparticles are single-phase with face-centered cubic (fcc) structure, and no phase of NiO or other impurity is observed. The peaks at $2\theta = 44.45^{\circ}, 51.73^{\circ}$ and 76.84° correspond to diffraction plane of Ni (111), Ni (200) and Ni (220) reflections, respectively (The international centre for powder diffraction data, powder diffraction files 2001). This result is subsequently confirmed by the TEM examination of the annealed sample where larger metallic Ni nanoparticles are clearly observed.

The bulk density of CF is 0.50 g cc^{-1} and on addition of Ni nanoparticles its density increases to 0.56 g cc^{-1} even at 1 wt% of nickel nanoparticles. The Ni nanoparticles are in magnetic behavior, but in CF its acts also as an electrical conductivity enhances. The Ni has affinity toward carbon and it forms Ni–C. The CF is heat treated to 1,000 °C, at this temperature graphitic structure does not develop and as a result it is in amorphous nature and it possesses combination of sp^2 and sp^3 hybridized carbon. The Ni can readily react with sp^3 bonded carbon and as a result sp^3 contribution in CF-Ni decreases. This has positive effect on the electrical conductivity. The electrical conductivity of CF is 50 S cm^{-1} which is due to the delocalized π electron in the carbon network while electrical conductivity of CF-Ni increases to 65 S cm^{-1}, this is due to the increases in sp^2 carbon content in it as compared to CF.

The mechanical strength is one of the essential requirements of CF because compressive forces are often encountered during its application as structural component. Therefore, compressive strength of CF should be sufficient to avoid any form of structural damage. The compressive strength of CF depends mainly on two factors namely microstructure and bulk density. It is observed that the compressive strength of CF is 7.0 ± 1 MPa and that of CF-Ni is 8.8 ± 1.2 MPa. This enhancement in strength is related to increase in bulk density and decrease in stress concentration center.

Figure 3 depicts the SEM micrographs of CF and CF-Ni. In case of CF, cells of the different sizes and distributions of cells are not uniform (Fig. 3a). The cell walls (i.e., ligaments) are broken during machining of samples for SEM characterization because of the brittle and porous nature of material (Kumar et al. 2013a, b, c). Figure 3b, SEM image of CF-Ni, in which the brightness of the surface increases due to the increase in electrical conductivity of CF-Ni by catalytic carbonization. The Ni nanoparticles are embedded in bulk carbon as well as on the surface and pore walls. Figure 3c shows magnified view of the pore walls in which

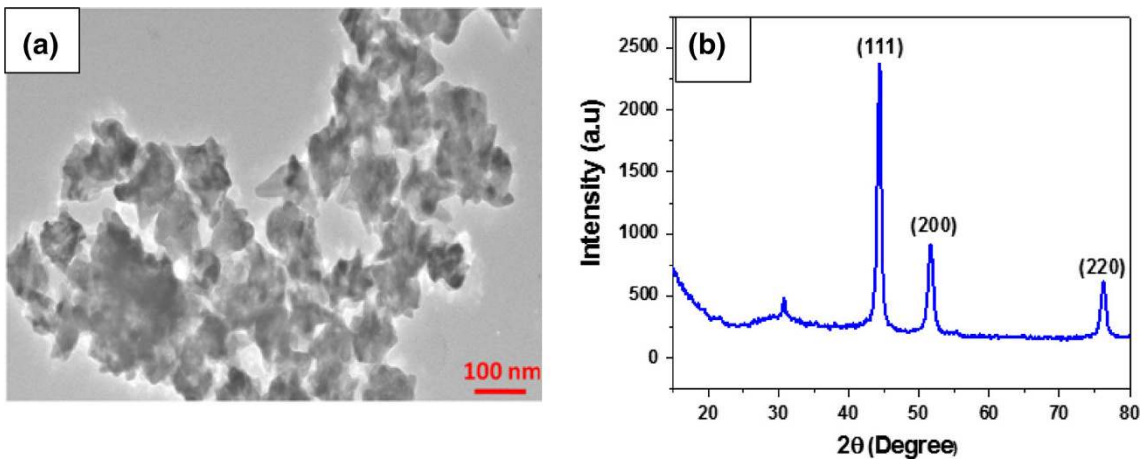

Fig. 2 **a** TEM micrograph and **b** XRD spectra of Ni nanoparticles

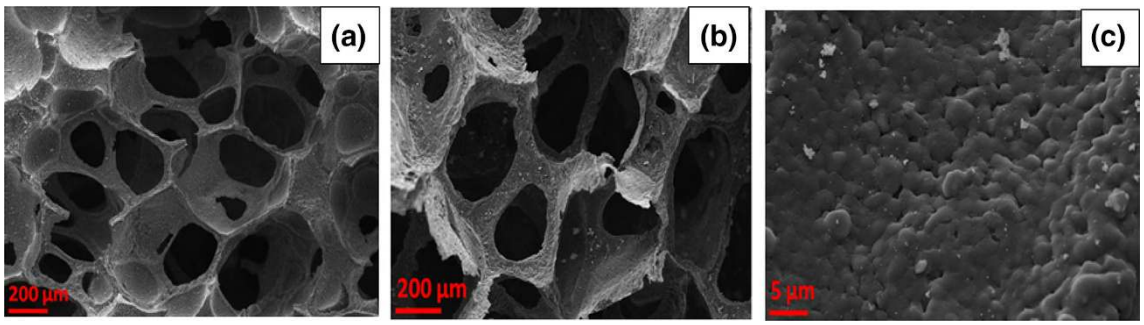

Fig. 3 SEM micrographs of **a** CF, **b** CF-Ni, **c** Ni nanoparticles embedded with carbon on the surface

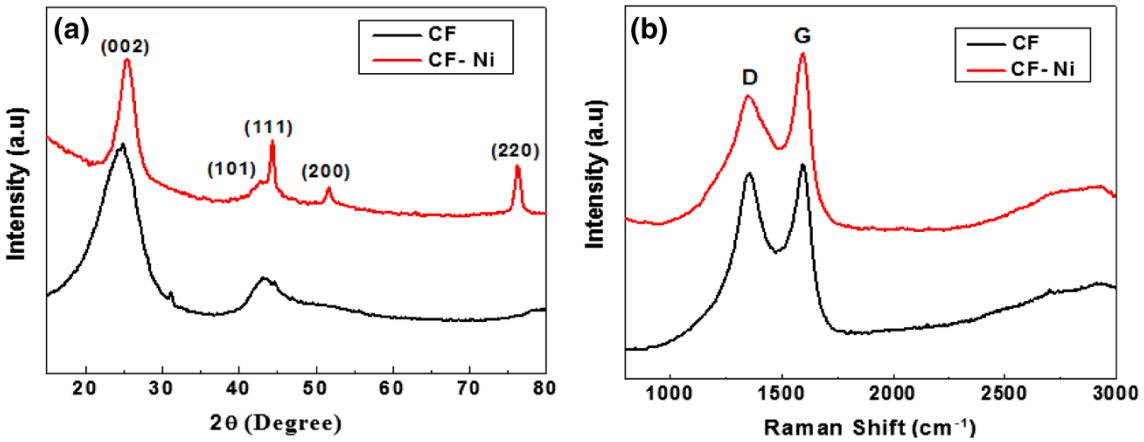

Fig. 4 **a** XRD spectra and **b** Raman spectra of CF and CF-Ni

embedded Ni nanoparticles are visible because the melting point of Ni is well above 1,400 °C.

Figure 4a shows the XRD spectra of CF and CF-Ni. In case of CF, there are two prominent peaks at $2\theta = 24.85$ and 43.15°, which correspond to the carbon of (002) and (101) diffraction plane. The XRD spectra of CF-Ni consist of peaks at $2\theta = 25.55°$, 42.76°, 44.45°, 51.77° and 76.35° corresponding to carbon (002) and (101), Ni crystal lattice (111), (200), and (220) planes. In case of CF-Ni, the 002 peak appears at higher diffraction angle. This suggests, Ni nanoparticle reacts with carbon, it acting as catalyst in improving the crystallite structure of carbon. The catalytic effect of carbon influences the structure in which sp^2 hybridization content increases. This also confirmed by Raman spectroscopy investigation. Figure 4b shows the Raman spectra of CF and CF-Ni and illustrates common features in the Raman shift 1,000–3,000 cm^{-1} region, the G, D and 2D band which lies at around 1,560, 1,360 and 2,700 cm^{-1}, respectively. The G band corresponds to the E 2 g phonon at the Brillion zone center. The D band is due to the breathing modes of sp^2 atoms and requires a defect for its activation and it only gives knowledge to the amount of disorder in the given structure (Ferrari and Robertson 2000; Dhakate et al. 2011). Figure 3b shows the Raman spectra of CF and CF-Ni, consisting of two bands D and G appearing at Raman shift 1,350 and 1,598 cm^{-1}, respectively. In case of CF, both bands almost appear at same intensity suggest the amorphous-type carbon while in case CF-Ni the G band intensity is higher as compared to D band. This suggests the structure of carbon modified with addition of Ni. The intensity ratio of D and G peak, i.e., (ID/IG) gives idea of defect level in the structure of CF, i.e., sp^3 bonded carbon. The ID/IG ratio in CF is higher this may be due to the presence of lesser amount sp^2 bonded carbon i.e., more defects. The CF has ID/IG ratio 0.9645 while in case of CF-Ni it decreases to 0.7065. This demonstrates that the Ni embedded in CF has positive effect on ID/IG ratio. The results of XRD and Raman spectroscopic are in agreement with each other and support the electrical conductivity data.

Electromagnetic shielding can be explained by measuring SE in terms of reflection and absorption losses. The SE of any shield material is the capacity to attenuate EM radiation that can be expressed in terms of ratio of incoming (incident) and outgoing (transmitted) power (Yong et al. 2005). The EM attenuation offered by a shield may depend on the three mechanisms: reflection of the wave from the front face of shield, absorption of the wave

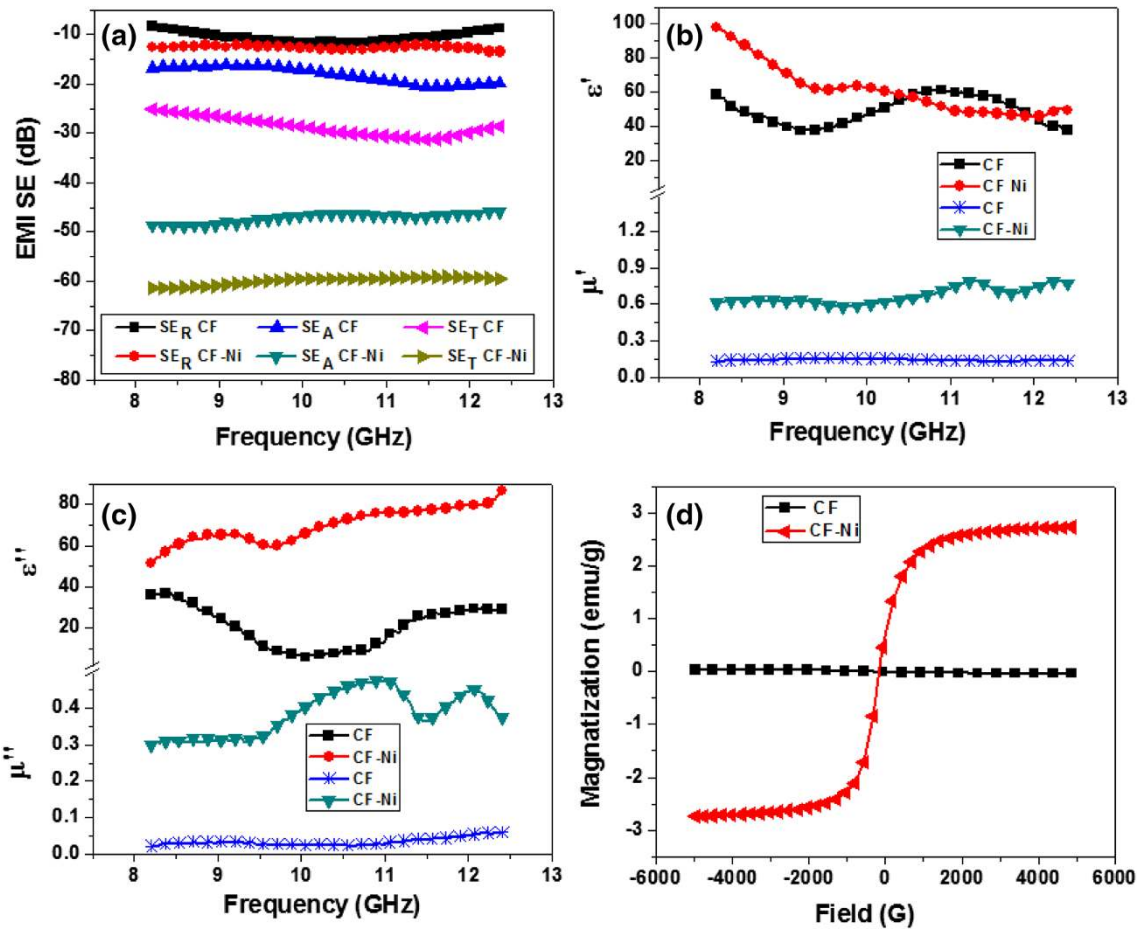

Fig. 5 **a** EMI SE SE_A, SE_R, SE_T of CF and CF-Ni, **b** Real permittivity and permeability (ε',μ'), **c** imaginary permittivity and permeability (ε'',μ'') and **d** room temperature magnetization plot of CF and CF-Ni

as it passes through the shield and multiple reflections of the waves at various interfaces (Han and Wang 2007). Therefore, SE is endorsed to three types of losses, i.e., reflection loss (SE_R), absorption loss (SE_A) and multiple reflection losses (SE_M) and can be expressed (Eq. 1) as:

$$SE_T(dB) = SE_R + SE_A + SE_M = 10\log(P_t/P_i) \quad (1)$$

where P_i and P_t are power of incident and transmitted EM waves, respectively. As, P_t is always less than P_i, therefore, SE is a negative quantity such that a shift towards more negative value means increase in magnitude of SE. It is important to note that the losses associated with multiple reflections can be ignored ($SE_M \sim 0$) in all practical cases when achieved SE_T is more than -10 dB. Therefore, SE_T can be expressed as (Eq. 2)

$$SE_T(dB) = SE_R + SE_A \quad (2)$$

Figure 5a shows the EM-SE of CF and CF-Ni in the X-band (8.2–12.4 GHz) frequency region. It is observed that total shielding effectiveness (SE_T) varies with frequency in both the cases. The value of SE_T for CF is 25 ± 3 dB while that of CF-Ni is 61 ± 5 dB. It is interesting to note that in CF-Ni, SE_T is more than double to that of CF. In case of CF, the SE_T is shared in ratio of reflection:absorption losses::1:2, i.e., reflection losses are -8.5 ± 2 dB and absorption losses are -16.86 ± 1 dB. While in CF-Ni, SE_T is governed by absorption losses (-48.5 ± 4 dB) and partially shared by reflection losses ($SE_R = -12.4 \pm 1$ dB).

The enhancement in the reflection components from -8.5 dB to 12.4 dB in case of CF-Ni is due to the increase in the electrical conductivity of CF-Ni as discussed in earlier section. While absorption losses enhancement from 16.86 to -48.5 dB in CF-Ni is due to the magnetic properties of material. Furthermore, in CF-Ni, Ni particles of size 200–300 nm on the surface of CF and embedded in CF provide higher surface and large interfacial area because of high aspect ratio of nanoparticles, which further enhances the SE due to the absorption.

To probe further, EM parameters which are responsible for EM radiation absorption, relative complex permittivity ($\varepsilon^* = \varepsilon' - i\varepsilon''$) and relative complex permeability

($\mu^* = \mu' - i\mu''$) of CF were measured in the frequency region 8.2–12.4 GHz to correlate with shielding properties. These complex parameters have been estimated from experimental scattering parameters (S_{11} and S_{21}) by standard Nicholson–Ross and Weir theoretical calculation (Nicolson and Ross 1970; Singh et al. 2012). The estimated real part of the EM parameters (ε', μ') is directly associated with the amount of polarization occurring in the material which symbolizes the storage ability of the electric and magnetic energy, while imaginary part (ε'', μ'') signifies the dissipated electric and magnetic energy. From Fig. 5b and c, it is clearly demonstrated that both real and imaginary parts of the permittivity (ε', ε'') vary with frequency. The real permittivity in CF is lower as compared to the CF-Ni and it decreases with increasing the frequency in CF-Ni.

The imaginary permittivity in CF-Ni increases with increasing the frequency (Fig. 5c). The decreasing permittivity in CF-Ni with frequency could be ascribed to the decreasing capability of the dipoles to sustain the in-phase movement with speedily pulsating electric vector of the incident radiation. According to EM theory (Colaneri and Shacklette 1992; Das et al. 2000), the ac conductivity (σ_{ac}) and skin depth (δ) are related to the imaginary permittivity (ε''), frequency (ω) and real permeability (μ') as $\sigma_{ac} = \omega\varepsilon_o\varepsilon''$, ($\sigma = \sigma_{ac} + \sigma_{dc}$) and $\delta = \sqrt{2/\sigma_{AC}\omega\mu'}$ which gives reflection (SE_R) and absorption losses (SE_A) as:

Reflection loss (SE_R) as

$$SE_R(dB) = 10\log\{\sigma_{ac}/16\omega\varepsilon_0\mu'\} \quad (3)$$

and absorption loss (SE_A) as

$$SE_A(dB) = 20\{t/\delta\}\log e = 20d\sqrt{\mu\omega\sigma_{ac}/2}\log e = 8.68\{t/\delta\} \quad (4)$$

$$SE_A(dB) = 8.68t\sqrt{\sigma\omega\mu'/2} \quad (5)$$

From the Eq. (3), it deduces that SE_R is related to frequency (ω), conductivity (σ_{ac}) and real permeability while the ac conductivity ($\sigma_{ac} = \omega\varepsilon_o\varepsilon''$) depends upon the frequency and imaginary permittivity (ε''). As shown in Fig. 5b, real permeability increases with increasing the frequency and it is maximum in case of CF-Ni and minimum in CF. While imaginary permittivity (Fig. 5c) also varies with frequency and it is minimum in case of CF and maximum in CF-Ni. This clearly demonstrates that SE_R is minimum in cases of CF and maximum in CF-Ni due to the higher value of electrical conductivity and imaginary permittivity. The higher value of imaginary permittivity does not store energy, but stored energy will be converted into thermal energy inside the material, which attenuates the EM radiation instead of just storing it. The carbon can easily dissipate the thermal energy due to its high value thermal conductivity.

Equation (5) shows that SE_A depends upon thickness, real permeability, frequency and conductivity of the shield material, from Fig. 5b, maximum real permeability is in case of CF-Ni as compared to CF where thickness is same in both the cases.

In case of CF-Ni, the existence of interfaces between Ni nanoparticles and carbon is responsible for interfacial polarization which further contributes to dielectric losses. Interfacial polarization occurs in heterogeneous materials due to the accumulation of charges at the interfaces and the formation of large dipoles. The magnetic nanoparticles act as tiny dipoles which get polarized in the presence of EM field and as a result better absorption.

The real permeability value of CF-Ni is more as compared to than that of CF (Fig. 5b). This is due to the improvement of magnetic properties along with the parallel reduction of eddy current losses since embedded Ni nanoparticles in magnetic behavior. In the X-band frequency region, the natural resonances can be attributed to the small size Ni particles in CF. Anisotropy energy of the small size materials, especially in the nanoscale, would be higher due to the surface anisotropic field effect of smaller material (Leslie-Pelecky and Rieke 1996). The higher anisotropy energy is also contributed in the enhancement of the EM radiation absorption.

The real and imaginary parts of complex permeability increase with increasing frequency in CF-Ni and maximum at frequency $\sim$11 GHz. While in the CF, it is very small due to the non-magnetic behavior. The magnetic nanoparticles embedded in the CF lead to better matching of input impedance along with the reduction of skin depth. This is attributing further in the increase of absorption losses of CF-Ni. This fact also varied by measuring the saturation magnetization of the CF and CF-Ni. Figure 5d shows the room temperature magnetization plot of CF and CF-Ni. The data of magnetization reveal that CF does not show any magnetization though out the magnetic field because carbon is non-magnetic in nature. However, CF-Ni shows the magnetization that displays narrow hysteresis loop. The CF-Ni possesses saturation magnetization 2.5 emu g^{-1} at 4.9 kg. These results are in agreement with results of electromagnetic attributes. This clearly demonstrates that even small amount of magnetic nanoparticles embedded in conducting CF is very much effective for absorption of EM radiation due to its large surface area and its magnetic properties.

Conclusions

In this investigation, Ni nanoparticle-embedded CF is developed by sacrificial template technique from a mixture

coal tar pitch and Ni nanoparticles. It reveals that addition of Ni nanoparticles in the CF influences electrical conductivity, complex permittivity and permeability, mechanical strength and EM-SE. The Ni nanoparticles are magnetic in nature, even though addition of nanoparticles improved the electrical conductivity of CF. This is due to catalytic effect of Ni nanoparticle in the carbon material which is revealed by XRD and Raman studies. The enhancements in electrical conductivity not significantly influence the EM-SE by reflection losses, but it is dominated by absorption of EM radiations due to the magnetic properties and large surface area of nanoparticles. Results of interfacial polarization occur in heterogeneous material (Ni nanoparticle-embedded CF). The shielding effectiveness of Ni nanoparticle-embedded CF increases by 144 % and absorption losses by 170 %. In addition to this, compressive strength of the CF increases from 7 to 8.8 MPa. This clearly demonstrates that the addition of small amount of magnetic nanoparticles in CF can be useful as EM radiation or radar absorbing material which can be used for stealth technology in civil and military applications.

Acknowledgments Authors are highly grateful to Director, NPL and Dr. R.B. Mathur for his kind permission to publish the results. Also thankful to Mr. Jai Tawale and Dr. K.N. Sood for doing SEM. Dr. R.P. pant for XRD, Dr. S.K. Dhawan for Shielding properties measurements and Dr. R.K. Kotnala for VSM.

References

Blacker JM, Plucinski JW (2011) Electrically graded carbon foam, US,7,867,608 B2

Che R, Peng LM, Duan XF, Chen Q, Liang X (2004) Microwave absorption enhancement and complex permittivity and permeability of Fe encapsulated within carbon nanotubes. Adv Mater 16(5):401–405

Che R, Zhi C, Liang C, Zhou X (2006) Fabrication and microwave absorption of carbon nanotubes/CoFe 2 O 4 spinel nanocomposite. Appl Phy Lett 88(3):033105–3

Chung DDL (2000) Materials for electromagnetic shielding. J Mater Eng Perform 9:350–354

Colaneri NF, Shacklette LW (1992) EMI shielding measurements of conductive polymer blends. IEEE Trans Instrum Meas 41:291–297

Coleman JN, Khan U, Blau JW, Gunko YK (2006) Small but strong: a review of the mechanical properties of carbon nanotubes-polymer composites. Carbon 44(9):1624–1652

Das NC, Das D, Khastgir TK, Chakraborthy AC (2000) Electromagnetic interference shielding effectiveness of carbon black and carbon fibre filled EVA and NR based composites. Compos A 31:1069–1081

Dhakate SR, Chauhan N, Sharma S, Tawale J, Singh S, Sahare PD, Mathur RB (2011) An approach to produce single and double layer graphene from re-exfoliation of expanded graphite. Carbon 49(6):1946–1954

Du F, Ma Y, Lv X, Huang Y, Li F, Chen Y (2006) (2006) The synthesis of single-walled carbon nanotubes with controlled length and bundle size using the electric arc methods. Carbon 44(7):1327–1330

Fang Z, Cao X, Li C, Zhang H, Zhang J, Zhang H (2006) Investigation of carbon foams as microwave absorber: numerical prediction and experimental validation. Carbon 44(15): 3348–3378

Fang Z, Li C, Sun J, Zhang H, Zhang J (2007) The electromagnetic characteristics of carbon foams. Carbon 45(15):2873–2879

Ferrari AC, Robertson J (2000) Interpretation of Raman spectra of disordered and amorphous carbon. Phy Rev B 61:14095–14107

Gallego NC, Klett JW (2003) Carbon foams for thermal management. Carbon 41(7):1461–1466

Han X, Wang YS (2007) Effect of emulsion polymerization conditions on the electromagnetic properties of magnetic and conductive polyaniline nanoparticles. J Funct Mater Devices 13:529–536

Huang CY, Wu CC (2000) The EMI shielding effectiveness of PC/ABS/nickel-coated- carbon-fibre composites. Eur Polymer J 36(12):2729–2737

Inagaki M, Morishita T, Kuno A, Kito T, Hirano M, Suwa T et al (2004) Carbon foams prepared from polyimide using urethane foam template. Carbon 42(3):497–502

Jesse MB, Douglas JM, Carbon foam EMI shield, US 2008/0078576 A1

Klett J, Hardy R, Romine E, Walls C, Burchell T (2000) High-thermal-conductivity, mesophase-pitch-derived carbon foams: effect of precursor on structure and properties. Carbon 38:953–973

Klett JW, McMillan AD, Gallego NG, Burchell TD, Walls CA (2004) Effects of heat treatment conditions on the thermal properties of mesophase pitch-derived graphitic foams. Carbon 42:1849–1852

Kumar R, Dhakate SR, Saini P, Mathur RB (2013a) Improved electromagnetic interference shielding effectiveness of light weight carbon foam by ferrocene accumulation. RSC Adv 3:4145–4151

Kumar R, Dhakate SR, Mathur RB (2013b) The role of ferrocene on the enhancement of the mechanical and electrochemical properties of coal tar pitch-based carbon foams. J Mater Sci 48:7071–7080

Kumar R, Dhakate SR, Gupta T, Saini P, Singh BP, Mathur RB (2013c) Effective improvement of the properties of light weight carbon foam by decoration with multi-wall carbon nanotubes. Mater Chem A 1:5727–5735

Leslie-Pelecky DL, Rieke RD (1996) Magnetic properties of nanostructured materials. Chem Mater 18:1770–1783

Liu JR, Itoh M, MachidaK-I (2006) Magnetic and electromagnetic wave absorption properties of α-Fe/Z-type Ba-ferrite nanocomposites. Appl Phy Lett 88(6):062503–3

Micheli D, Marcheti M (2012) Mitigation of Human exposure to electromagnetic fields using carbon foam and carbon nanotubes. Engineering 4:928–943

Moglie F, Micheli D, Laurenzi S, Marchetti M, Primiani VM (2012) Electromagnetic shielding performance of carbon foams. Carbon 50:1972–1980

Nicolson AM, Ross GF (1970) Measurement of the intrinsic properties of materials by time-domain techniques, IEEE Trans. Instrum Meas 19:377–382

Oh JH, Oh KS, Kim CG, Hong CS (2004) Design of radar absorbing structures using glass/epoxy composites containing carbon black in X-band frequency ranges. Compos Par B Eng 35:49–56

Park KY, Lee SE, Kim CG, Han JH (2006) Fabrication and electromagnetic characteristics of electromagnetic wave absorbing sandwich structures. Compos Sci Technol. 66:576–584

Saravanan P, Jose TA, Thomas PJ, Kulkarni GU (2001) Bull. Mater Sci 24:515–521

Seo S, Chin WS, Lee DG (2004) Characterization of electromagnetic properties of polymeric composite materials with free space method. Compos Struct 66:533–542

Singh AP, Garg P, Alam F, Singh K, Mathur RB, Tandon RP, Chandra A, Dhawan SK (2012) Phenolic resin-based composite sheets filled with mixtures of reduced graphene oxide, -Fe2O3 and carbon fibers for excellent electromagnetic interference shielding in X-band. Carbon 50:3868–3875

The international centre for powder diffraction data, powder diffraction files, 2001, Card Number: JCPDS-040850

Wang H, Wang G, Li W, Wang Q, Wei W, Jiang Z, Zhang S (2012) A material with high electromagnetic radiation shielding effectiveness fabricated using multi-walled carbon nanotubes wrapped with poly(ether sulfone) in a poly(ether ether ketone) matrix. J Mater Chem 22:21232–21237

Yadav A, Kumar R, Bhatia G, Verma GL (2011) Development of mesophase pitch derived high thermal conductivity graphite foam using a template method. Carbon 49:3622–3630

Yang J, Shen ZM, Hao ZB (2004) Microwave characteristics of sandwich composites with mesophase pitch carbon foams as core. Carbon 42:1882–1885

Yang Y, Gupta MC, Dudley KL, Lawrence RC (2005) Novel carbon nanotube-polystyrene foam composites for electromagnetic interference shielding. Nano Lett 5(11):2131–2134

Yong Y, Gupta MC, Dudley KL, Lawrence RW (2005) Conductive carbon nanofiber- polymer foam structures. Adv Mater 17: 1999–2003